

The Resistive Nature of Decomposing Interfaces of Solid Electrolytes with Alkali Metal Electrodes

Juefan Wang and Abhishek A. Panchal

*Department of Materials Science and Engineering,
National University of Singapore, 9 Engineering Drive 1, 117575, Singapore*

Gopalakrishnan Sai Gautam

Department of Materials Engineering, Indian Institute of Science, Bangalore 560012, India

Pieremanuele Canepa

*Department of Materials Science and Engineering,
National University of Singapore, 9 Engineering Drive 1, 117575, Singapore and
Department of Chemical and Biomolecular Engineering,
National University of Singapore, 4 Engineering Drive 4, 117585, Singapore**

A crucial ingredient in lithium (Li) and sodium (Na)-ion batteries (LIBs and NIBs) is the electrolytes. The use of Li-metal (Na-metal) as anode in liquid electrolyte LIBs (NIBs) is constrained by several issues including thermal runaway and flammability, electrolyte leakage, and limited chemical stability. Considerable effort has been devoted toward the development of solid electrolytes (SEs) and all-solid-state batteries, which are presumed to mitigate some of the issues of Li-metal(Na-metal) in contact with flammable liquid electrolytes. However, most SEs, such as Li_3PS_4 , $\text{Li}_6\text{PS}_5\text{Cl}$ and Na_3PS_4 readily decompose against the highly reducing Li-metal and Na-metal anodes. Using first-principles calculations we elucidate the stability of more than 20 solid||solid interfaces formed between the decomposition products of Li_3PS_4 , $\text{Li}_6\text{PS}_5\text{Cl}$ (and Na_3PS_4) against the Li-metal (Na-metal) electrode. We suggest that the work of adhesion needed to form a heterogeneous interfaces is an important descriptor to quantify the stability of interfaces. Subsequently, we clarify the atomistic origins of the resistance to Li-ion transport at interfaces of the Li-metal anode and selected decomposition products (Li_3P , Li_2S and LiCl) of SEs, via a high-fidelity machine learned potential (MLP). Utilising an MLP enables nano-second-long molecular dynamics simulations on ‘large’ interface models (here with 8320 atoms), but with similar accuracy to first-principles approaches. Our simulations demonstrate that the interfaces formed between Li-metal and argyrodite (e.g., $\text{Li}_6\text{PS}_5\text{Cl}$) decomposition products are resistive to Li-ion transport. The implications of this study are important since binary compounds are commonly found in the vicinity of Li(Na)-metal upon chemical and/or electrochemical decomposition of ternary and quaternary SEs.

I. INTRODUCTION

Rechargeable lithium-ion batteries (LIBs) keep gaining importance for the development of the next-generation energy storage devices and electric vehicles because of their outstanding gravimetric and volumetric energy densities.[1–5] Lithium metal batteries (LMBs) utilizing Li-metal anodes—that can achieve unprecedented energy densities theoretically, as compared to LIBs—have become one of the central topics of current research in rechargeable batteries. [4–6] The primary challenge in constructing practical LMBs is stabilizing the Li-metal||electrolyte interface, with scientific studies mostly focused on identifying electrolyte formulations with limited reactivity and/or suitable additives.[1, 5, 7] Stabilizing the metal||electrolyte interface is also a bottleneck in developing Na-metal batteries (NMBs).[4, 5, 8–10]

Solid electrolytes (SEs) are critical components in the development of LMBs and solid-state LIBs.[11–18] Besides acting as separators between electrodes, SEs are also expected to alleviate some of the safety issues between Li-metal anodes and liquid electrolytes. [4, 5, 19] Nevertheless, numerous reports have demonstrated high

electrochemical instabilities of SEs when in contact with Li-metal anode (and other electrode materials).[4] For example, sulfur-containing SEs are unstable against Li-metal, resulting in the formation of undesired decomposition products, which may resist Li-ion transport and/or facilitate electron transport.[12–15, 20–22] Thus, the stabilization of interfaces formed between Li-metal (or other alkali-metal electrodes) and SEs remains a significant bottleneck in designing practical solid-state batteries.

Electrolyte decomposition occurs at small length scales away from the exteriors of the cell packs that constitute a battery. Therefore, the characterization of decomposition products in fully assembled and operating devices requires dedicated custom-made and expensive tools.[13, 14, 23, 24] A number of reports have analyzed the compositions, structures, and formation mechanisms of the decomposing products of SEs against metal electrodes(metal electrode||SE).[12–15, 20–22] For example, X-ray photoemission spectroscopy (XPS) experiments by Wenzel *et al.*[14] reported that $\text{Li}_6\text{PS}_5\text{X}$ (with $\text{X}=\text{Cl}$, Br and I), upon contact with Li-metal, forms Li_2S , LiX , and Li_3P . As a result, the decomposition products of metal electrode||SE are expected to be multiphased and highly

heterogeneous, which complicates the description of ionic transport across interfaces. Furthermore, the structures and properties of the metal electrode||SE interfaces are expected to be markedly different from the bulk materials. A detailed study of the interfacial properties, particularly ionic transport, is needed for the advancement of solid-state batteries.

Another aspect of solid-state batteries relates to the mechanical stability (i.e., adhesion) of the solid||solid interfaces that are electrochemically formed. The loss of contact due to lack of adhesion between Li-metal and SEs appears as a major cause driving the buildup of interfacial impedance in solid-state devices.[4, 5, 25] To evaluate the mechanical stabilities of the interfaces, Lepley and Holzwarth[26] have performed accurate first-principles calculations of several Li-metal||SE interfaces (such as, Li||Li₂O, Li||Li₂S, Li||Li₃PO₄ and Li||Li₃PS₄) and found that all interfaces were stable except Li||Li₃PS₄. Other studies have investigated the effects of stability of heterogeneous interfaces on the Li-ion transport properties.[27–29]

Yang and Qi[27] have proposed that an interface with good adhesion, i.e. "lithiophilic interface" can result in a faster critical stripping current density, which is crucial to prevent dendrite growth. Recently, Seymour and Aguadero[28] have shown that Li (or Na)-ion transport across alkali-metal||SE interfaces correlates directly with the interfacial adhesion. Yang *et al.*[29] have employed classical molecular dynamics (MD) to study the process of Li plating and stripping on solid Li₂O, showing that a coherent interface with strong interfacial adhesion and fast Li-ion diffusion can prevent pore formation at the interface. Here, we perform a systematic investigation including a larger data set of solid||solid interfaces, particularly focusing on the correlation between the atomistic structure of interfaces and ionic transport, which is presently lacking.

Further, we address the interfacial stability and Li-ion mobility of multiple interfaces formed between Li-metal electrode and decomposition products of topical SEs, such as, Li₃PS₄, [15, 26, 30, 31] argyrodite-Li₆PS₅Cl[14] and LiPON, with the general formula Li_xPO_yN_z. [23, 24, 32] We also analyze the Na||Na₂S and Na||Na₃P interfaces, which form upon the decomposition of Na₃PS₄ against Na-metal.[13] We perform large-scale MD simulations of selected interfaces, (i.e., Li||Li₃P, Li||Li₂S and Li||LiCl) based on high-fidelity machine learned potentials (MLPs) trained on accurate first-principles data, which carry the accuracy of *ab initio* molecular dynamics (AIMD) while give access to appreciably larger time and length scale simulations.

We reveal that the mechanical stabilities of the Li (or Na)-metal||SE interfaces are primarily governed by the atomistic structures of the interfaces, which in turn are dependent on the surface orientations and/or terminations of the decomposition products. Further, we show that the interfaces formed between Li-metal and decomposition products of the argyrodite Li₆PS₅Cl SE (i.e.,

Li₃P, Li₂S and LiCl) are resistive to Li-ion transport, explaining the observed impedance buildup. Our results provide insights to engineer solid||solid interfaces with better interfacial stability and improved ionic transport.

II. CONSTRUCTION OF INTERFACES OF DECOMPOSITION PRODUCTS AND METAL ANODES

We discuss the procedure to build heterogeneous interfaces between an alkali-metal (Li or Na) with one of their binary compounds (e.g., Li₃P), formed as a result of SE decomposition. In constructing the heterogeneous interfaces between the alkali-metal (e.g., Li or Na) and the binary compounds, we identify stable stoichiometric surfaces (following Tasker's criteria[33]) with low surface energies, γ , of both materials, which are paired into an interface (see Table S1 of the Electronic Supplementary Information, ESI). To describe γ , we have used the slab model in Eq. 1.[34]

$$\gamma = \lim_{N \rightarrow \infty} \frac{1}{2S} [E_{\text{slab}}^N - NE_{\text{bulk}}] \quad (1)$$

where S is the surface area of the slab, E_{slab}^N is the energy of the relaxed slab containing N formula units, and E_{bulk} is the energy per formula unit of the bulk structure. The energies of Eq. 1 (and the following equations) are Gibbs energies, which we approximate by density functional theory (DFT, see Sec. VII) total energies ignoring pV and entropic contributions. Slab models included sufficient number of layers and a vacuum of 15 Å to converge γ to within ± 0.01 J m⁻².

The set of stable surfaces in Li(or Na) metal and binary compounds considered, and their corresponding γ , are displayed in the Wulff shapes of Figure 1.[35, 36] γ values, not shown in Figure 1, are included in Table S2-S3 of ESI. The (100) surface of Li-metal has the lowest surface energy of ~ 0.46 J m⁻², while for Na-metal, the (100) and (110) surfaces have similar γ values, ~ 0.22 J m⁻² and ~ 0.21 J m⁻². In Li₂S, Li₂O, Na₂S, and Na₂O, the (111) facet dominates the Wulff shape, while for Li₃P, LiCl, Li₃N, and Na₃P, the {001}-type surfaces have the lowest γ (Figure 1). Our calculated surface energies, ~ 0.33 J m⁻² for the (111) surface and ~ 0.51 J m⁻² for the (110) surface of Li₂S, as well as ~ 0.53 J m⁻² for the (111) surface of Li₂O are consistent with previous literatures.[37, 38] Li₃N and LiCl exhibit stable facets that have both Li and anion species, while other compounds have stable facets exposing a Li (or Na) layer.

The surfaces of Figure 1 are subsequently paired to form heterogeneous interfaces. Different metrics serve to quantify the effect of mechanical strain and/or the chemical bond formation/destruction at the interface.[39, 40] The interface formation energy (E_f in Eq. 2) is the energy difference between the interface model and bulk structures of A and B , and includes both mechanical (i.e.,

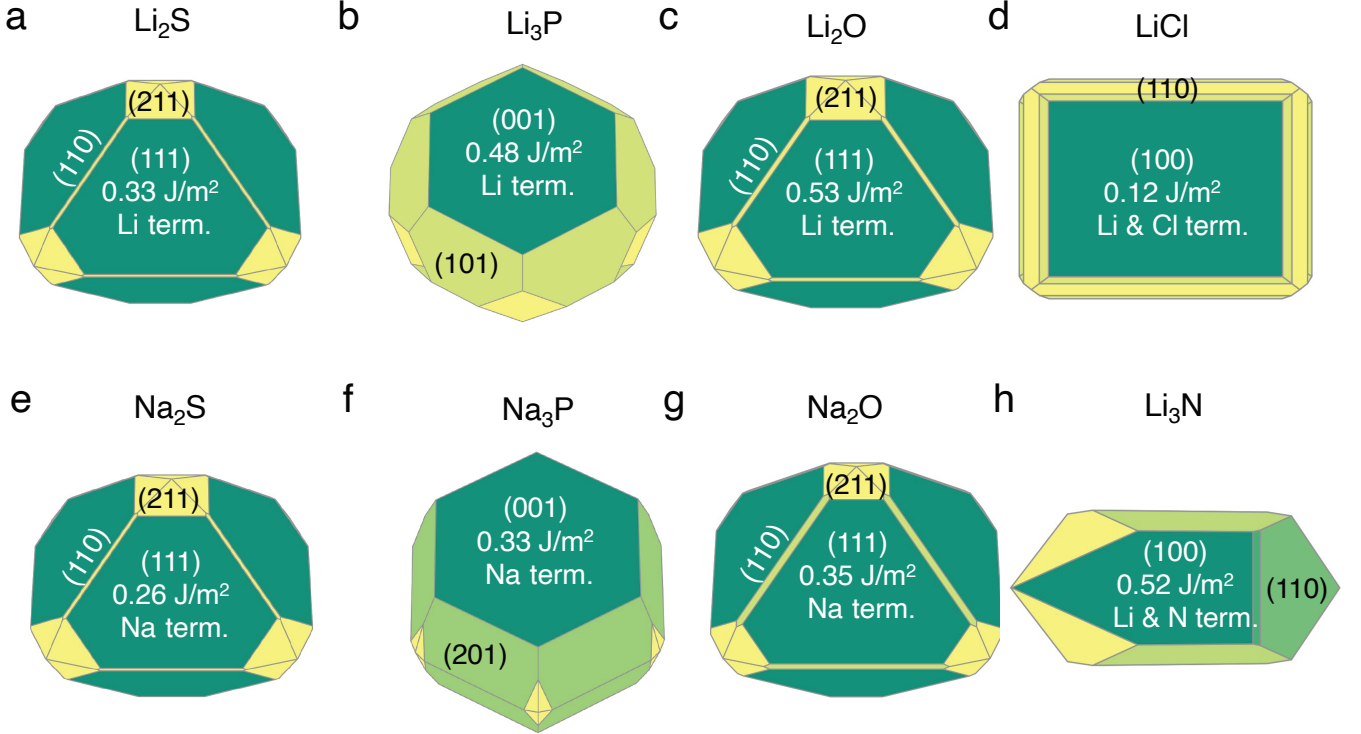


FIG. 1. Computed Wulff shapes of binary compounds Li_2S (panel a), Li_3P (b), Li_2O (c), LiCl (d), Na_2S (e), Na_3P (f), Na_2O (g), and Li_3N (h), with their corresponding surface energies (in J m^{-2}). The chemical nature of the surface terminations (term.) are indicated. Wulff polygons are constructed using stoichiometric, non-polar, and symmetric (including an inversion symmetry) surfaces.

elastic strain) and chemical components.[34]

$$E_f = \frac{E_{AB} - [N_A E_A + N_B E_B]}{2S} \quad (2)$$

where S is the surface area of the interface, E_{AB} is the energy of the fully relaxed interface model, containing N_A and N_B formula units of materials A and B , whose bulk energies are E_A and E_B . Elastic stress can arise in interfaces displaying large lattice mismatch, and "absorbed" by the interface through the release of the stress energy, via formation of dislocations.[41, 42] By removing the elastic strain from E_f (of Eq. 2), we obtain two important descriptors: *i*) the interfacial energy, σ of Eq. 3, and *ii*) the work of adhesion, W_{adhesion} of Eq. 4, which are paramount in evaluating the overall stability of interfaces. σ quantifies the formation (or destruction) of chemical bonds as the interface is created, excluding all mechanical contributions.

$$\sigma = \frac{E_{AB} - [N_A E_{A(z)} + N_B E_{B(z)}]}{2S} \quad (3)$$

where $E_{A(z)}$ and $E_{B(z)}$ are the energy per formula unit of the bulk A and B , as obtained from a constrained relaxation along the normal direction (z) to the interface, where the in-plane lattice vectors of the bulk structures are fixed to those of the fully relaxed interface. It fol-

lows that, the elastic strain energy associated with the interface is calculated as $E_f - \sigma$.

The work of adhesion, W_{adhesion} (of Eq. 4) is the work done to part two adherent surfaces to an infinite distance, and quantifies the mechanical stability of an interface.

$$W_{\text{adhesion}} = \gamma_A + \gamma_B - \sigma \quad (4)$$

where γ_A and γ_B (Eq. 1) are the surface energies of materials A and B . Nominally, small (positive) values of σ and large (positive) values of W_{adhesion} are indicative of high interfacial stability. To account for the effect of elastic strain, Eq. 5 gives an alternative definition of W_{adhesion}

$$W_{\text{adhesion}} = \gamma_A + \gamma_B - E_f \quad (5)$$

For creating interface models, we use the algorithm by Taylor *et al.*,[43] which samples the configurational space to find interface models that minimize the lattice mismatch between two materials. While pairing surfaces, we used the in-plane lattice constants of the binary compounds (e.g., Li_3P) and applied a lattice mismatch-induced strain to the metal surface, since the bulk moduli of binary compounds are typically greater than the alkali-metals (i.e., Li and Na).[11, 44] The constructed interface models are symmetric; for example, $\text{Li}_2\text{S}||\text{Li-metal}$ consists of two identical interfaces that forms a $\text{Li}_2\text{S}||\text{Li-metal}||\text{Li}_2\text{S}$ system, as displayed in panels c and

d in Figure 2. The slab thickness of binary compounds is typically ~ 10 Å, which is sufficient to distinguish the interface features from their bulk-like properties. However, thicker slabs are required for Li (~ 12 Å) and Na (~ 14 Å) to distinguish the interface regions from the bulk region. [26]

III. STABILITY OF INTERFACES OF DECOMPOSITION PRODUCTS AND METAL ELECTRODES

Figure 2a and b show the computed interfacial energetics, E_f , σ , and W_{adhesion} (as defined in Eq. 4), for a number of interfaces considered. An illustration of the interface models for Li(110)||Li₂S(110) and Na(110)||Na₂S(110) is shown in Figure 2c and d, where the interfacial regions are indicated by the shaded areas. Representations of other interfaces are shown in Figure S1-S5 of ESI. In the Li cases considered, we find the most stable interfaces are those formed with Li₃N, displaying W_{adhesion} in the range of 0.8–1.0 J m⁻², and $\sigma \sim 0.25$ J m⁻² (Figure 2a). In contrast, the least stable interfaces are Li||LiCl, which exhibit low W_{adhesion} and high σ . In Na-based systems, the most and least stable interfaces are Na(110)||Na₂O(110) and Na(100)||Na₃P(001), respectively. Note that results of W_{adhesion} from Eq. 5 (including strain contributions) in Figure S7-S8 appear similar in magnitude (and sign) to those obtained with Eq. 4 (excluding strain) in Figure 2. Therefore, we will refer to W_{adhesion} of Eq. 4 and Figure 2 through the remainder of the manuscript.

Previous computational and experimental studies have suggested that Li||Li₂S, Li||Li₃P and Li||LiCl interfaces are expected to form when argyrodite-Li₆PS₅Cl SE reacts with Li-metal.[14, 15] A comparison of W_{adhesion} (Figure 2a) of these interfaces indicates Li||LiCl \ll Li||Li₂S $<$ Li||Li₃P. Li(100)||Li₃P(001) is expected to dominate the overall interface of Li-metal and Li₆PS₅Cl, if similar quantities of Li₂S and Li₃P are produced upon decomposition. In the case of Li₃PS₄, predicted values of W_{adhesion} (Figure 2a) suggest the coexistence of both Li||Li₂S and Li||Li₃P interfaces, consistent with prior literature.[15, 45, 46] For LiPON, W_{adhesion} follows the order Li||Li₃P \ll Li||Li₂O \approx Li||Li₃N, implying that the Li-metal anode will mostly interface with Li₂O and Li₃N, also consistent with previous investigations.[15, 23, 24, 32, 47]

In most cases considered, the interfacial region (shaded regions in Figure 2c and d) exhibits substantial atomic rearrangements upon full relaxation, with the exceptions being Li(110)||Li₃N(110) (Figure S3) and Li(110)||LiCl(100) (Figure S2). A qualitative analysis of the interface models suggests that there is always a pronounced atomic reconstruction on the metal side of the interface as compared to that of the binary compound for all Li (and Na) interfaces. This is another confirmation that both Li and Na metals are softer than their binary

compounds.[44] Li (or Na) atoms originating from the metal side of the interfacial region form stabilising bonds with anion species from the compound side, with bond lengths that are similar to the bulk binary structures (see Table S5).

In general, interfaces with lattice mismatch smaller than a few percent can be considered as epitaxial, and the re-organization of atoms at the interface remains minimal compared to others with significant lattice mismatch ($\geq 5\%$). In some cases, we find large lattice mismatches when interfaces are formed from the dominant facets of binary compounds with the (100) or (110) surfaces of the metals (Li or Na). For example, the Li₂S(111) facet displays a $\sim 14.2\%$ lattice mismatch with the Li(100) surface (Table S3), indicating that such an interface may not occur practically. The lattice mismatch between Li₂S(110) and Li(110) facets is lower ($\sim 5.1\%$) and consequently exhibits higher W_{adhesion} than Li₂S(111)||Li(100). The Li₂S||Li interface is likely to exhibit significant structural re-arrangement since Li₂S(110) facet does not occupy a significant portion of the Wulff volume of Li₂S, and consequently result in a Li₂S||Li interface that is susceptible to delamination in real devices.

We also find that the surface terminations of binary compounds are crucial to determine the interfacial stability. For example, the Li(110)||Li₂O(111) interface has a small lattice mismatch of $\sim 1.73\%$ (Table S3). However, its fully relaxed geometry exhibits larger lattice distortion of the interfacial region as compared to other Li||Li₂O based interfaces (see Figure S4). This interfacial instability comes from the fact that the Li₂O(111) surface is terminated with only Li atoms —this excess number of Li atoms and lack of anions near the interface region affects the chemical stabilization of the interface due to the lack the bond formation between Li (from the metal side of the interface) and O.

In Na systems, the Na(110)||Na₂S(110), Na(100)||Na₂S(111), and Na(100)||Na₃P(001) show reconstructions in the interfacial region similar to their Li analogues (Figure 2c and Fig. S1c,d). Additionally, we find the computed values of W_{adhesion} (and σ) to be lower (less positive) than their corresponding Li analogues (see Figure 2a and b). Despite the low values of W_{adhesion} (< 0.35 J m⁻²), both Na||Na₂S and Na||Na₃P may still occur at the Na-metal electrode. The Na||Na₂O interface has a significantly larger W_{adhesion} (~ 0.65 J m⁻²) than Na||Na₃P (~ 0.35 J m⁻²) and Na||Na₂S interfaces (~ 0.30 J m⁻²).

IV. LITHIUM TRANSPORT AT HETEROGENEOUS INTERFACES

To quantify ion transport through heterogeneous interfaces, we have used the tracer diffusivity, D^* of Eqs. 6 and 7. While we quantify only Li-ion transport across heterogeneous interfaces, similar qualitative trends might hold

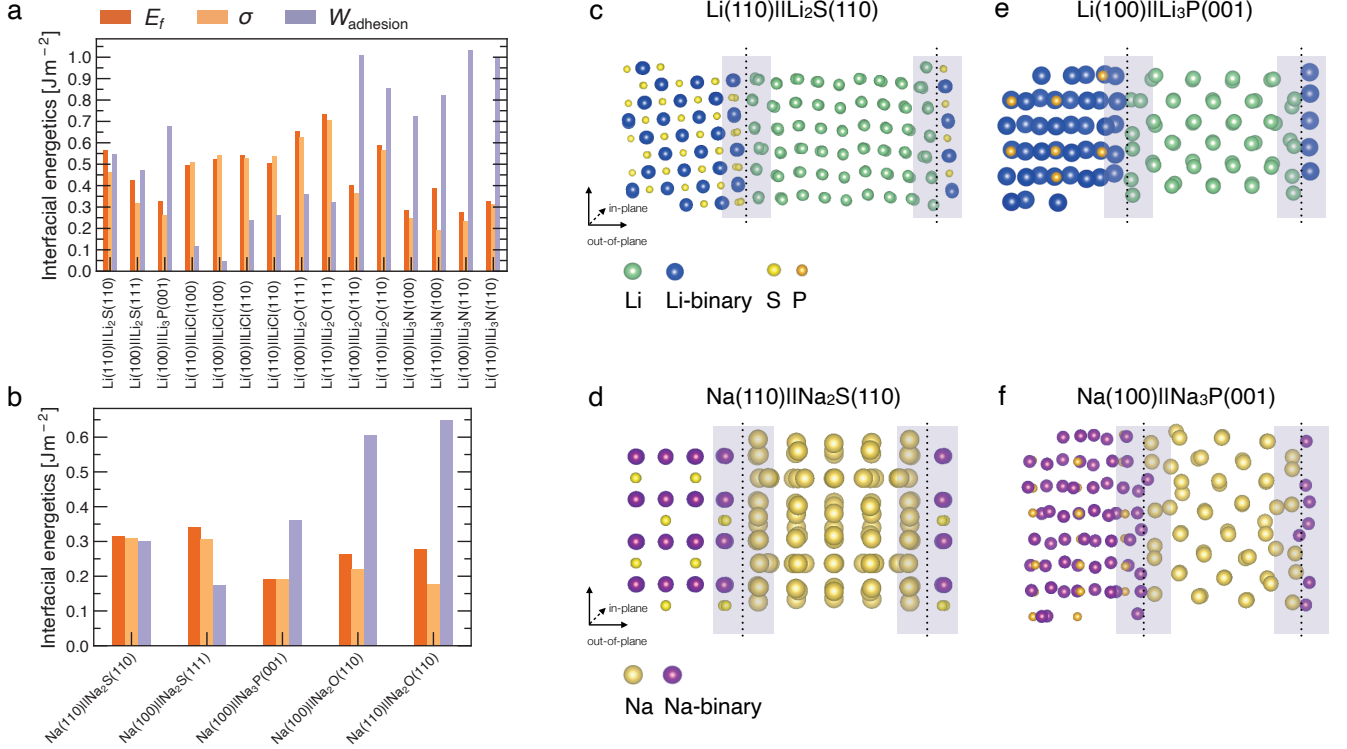


FIG. 2. Computed interfacial quantities (in J m^{-2}) for (a) Li-based interfaces and (b) Na-based interfaces. Atomic structures of representative interfaces, namely (c) $\text{Li(110)||Li}_2\text{S(110)}$, (d) $\text{Na(110)||Na}_2\text{S(110)}$ (e) $\text{Li(100)||Li}_3\text{P(001)}$ and (f) $\text{Na(100)||Na}_3\text{P(001)}$. The interface regions are indicated by shaded areas. The non-periodic direction of the interface is indicated by the “out-of-plane” vectors.

for Na-ion transport as well.

$$D^*(T) = \lim_{t \rightarrow \infty} \frac{1}{2dt} \frac{1}{N} \sum_{i=1}^N \langle |r_i(t) - r_i(0)|^2 \rangle; \quad (6)$$

$$D^*(T) = D_0 \exp \left[-\frac{E_a}{k_B T} \right]. \quad (7)$$

where $r_i(t)$ is the displacement of the i^{th} Li-ion at time t , N is the number of diffusing ions, and d is the dimensionality of the diffusion process. E_a in the Arrhenius Eq. 7 is the Li-ion migration energy, D_0 is the ionic diffusivity at infinite temperature (T), and k_B is the Boltzmann constant. We obtain D^* , D_0 and E_a from MD simulations based on our trained MTPs,[48] which is machine learned from AIMD simulations of the bulk and interface structures (see Sec. VII B). The largest MD simulations of heterogeneous interfaces investigated in this study contains 8320 atoms and samples the ion dynamics for times >10 ns, which enables an accurate assessment of transport properties. Table S6 summarizes the mean absolute errors from the MTP training and its validation.

The calculated D^* as a function of temperature for bulk binary compounds Li_2S , Li_3P and LiCl , with and without Li^+ vacancies (Vac) are shown in Figure 3. The assessment of Li-ion transport in the bulk structures of Li_2S , Li_3P and LiCl is crucial to compare the transport

across the heterogeneous interfaces. Notably, our calculated E_a is in reasonable agreement with experimental results (see Table S7). For example, the calculated E_a in LiCl with Vac, $\sim 399 \pm 5$ meV, is qualitatively similar to the existing experimental value (~ 510 meV[49]). The computed E_a of Li_3P with Vac ($\sim 155 \pm 7$ meV) is in better agreement with experiment (~ 180 meV[50]) as compared to the pristine Li_3P ($\sim 1061 \pm 53$ meV). On the other hand, the calculated E_a in pristine- Li_2S ($\sim 1573 \pm 104$ meV) is closer to the experimental value (~ 1.5 eV at $T \lesssim 800$ K[51]) than the calculated E_a in Li_2S with Vac ($\sim 313 \pm 2$ meV). Unsurprisingly, the introduction of Vac lowers the activation energies of both Li_2S and Li_3P as shown in Figure 3. The calculated E_a of Li_3P (with Vac) is lower than that of Li_2S (with Vac), which is in agreement with previous studies showing superior Li-ion conductivity of Li_3P over Li_2S . [52]

To investigate the Li-ion transport across the argyrodite- $\text{Li}_6\text{PS}_5\text{Cl||Li-metal}$ interface (i.e., the decomposition products of argyrodite with Li metal), we performed MTP-MD simulations on three interface models, namely, $\text{Li(110)||Li}_2\text{S(110)}$, $\text{Li(100)||Li}_3\text{P(001)}$ and $\text{Li(110)||LiCl(100)}$. The choice of these specific interfaces is motivated by their larger W_{adhesion} values (Figure 2a) compared to other possible configurations using Li-metal and the same binary compound. We randomly introduced a number of Li^+ vacancies ($\sim 1.1\%$) in the

interface region to calculate D^* , since it is likely that heterogeneous interfaces will comprise highly defective materials, especially due to the *in situ* formed decomposition products. To distinguish Li^+ belonging either to Li-metal or binary compounds, we have labeled Li^+ in Li-metal as $\text{Li}^+(\text{metal})$ (green spheres in Figure 4, Figure S9), and Li^+ in binary compounds as $\text{Li}^+(\text{binary})$ (dark blue spheres), respectively. Furthermore, the direction of Li-ion transport with respect to the interfacial plane, i.e., in-plane or out-of-plane, helps to qualify the nature of Li transport. Indeed, only Li-ion diffusing out-of-plane will contribute to effective ion-transport across the interface. The predicted Li^+-D^* in both Li-metal and binary compounds are summarized in Table S8. The mean square displacement (MSD) plots used to derive the Li^+-D^* are shown in Figures S10-S12.

In Figure 4a-d and Figure S9a-b, we show the snapshots of different interfaces at 400 K during the MTP-MD simulations. In the following paragraphs, bulk is intended as the portion of the interface model which mimics the bulk structure. Initially, all interfaces exhibit modest atomic rearrangements near the interface region (violet shaded area). After ~ 5 ns, significant Li^+ displacement in both the metal and binary bulk along with Li^+ exchange (i.e., there is a significant amount of $\text{Li}^+(\text{metal})$ diffusing into Li_3P bulk and vice-versa) can be clearly observed in $\text{Li}(100)||\text{Li}_3\text{P}(001)$. This can be understood by the high values of Li^+-D^* (Figure 4e) in both the in-plane (within bulk systems, 3.03×10^{-6} –

3.76×10^{-6} cm^2/s) and out-of-plane (across the bulk systems, 1.93×10^{-7} – 1.99×10^{-7} cm^2/s) directions in the $\text{Li}(100)||\text{Li}_3\text{P}(001)$ system.

In contrast, in $\text{Li}(110)||\text{Li}_2\text{S}(110)$ and $\text{Li}(110)||\text{LiCl}(100)$, we observe limited diffusion events and sparse exchange of Li-ions during the MTP-MDs, which in turn is quantified by the low in-plane (4.86×10^{-8} – 1.89×10^{-7} cm^2/s) and even lower out-of-plane (6.43×10^{-9} – 2.21×10^{-8} cm^2/s) diffusivities in both systems. We find that for all interfaces, the out-of-plane components of both $\text{Li}^+(\text{metal})$ and $\text{Li}^+(\text{binary})$ are much smaller than their respective in-plane components, which indicate that the Li^+ diffusion across the interface remains limited.

V. DISCUSSION

A systematic study of the structures, interfacial energetics, and ionic transport properties of solid/solid interfaces is paramount for the development of solid-state batteries. Here, we have used a combination of accurate DFT calculations to explore the stability of interfaces arising from the decomposition of SEs with highly reducing alkali-metals, i.e., Li and Na. Upon identifying the thermodynamically stable heterogeneous interfaces, we trained MTPs based on accurate AIMD simulations, and in turn used such MTPs to run long duration (>10 ns) simulations to elucidate the Li-ion transport properties across specific interfaces.

Although the morphology of real electrode||SE interfaces can be far more complex than the interface models used here, our detailed atomistic models provide insights of the microscopic structure and mechanical stability of buried interfaces between SEs and alkali-metals. Still one major limitation of our analysis is the finite number of interface models considered (20 in this study). Clearly, it is not possible to survey the whole configurational space of interfaces (potentially thousands[11, 16, 34]), and alternative strategies should be sought.

This study demonstrates that both surface orientations together with the surface terminations of binary compounds can largely affect the atomistic structures of interfaces (see Section 3), which in turn determine the interfacial lattice coherence, the thermodynamic stability of interfaces and the mechanical stability of such interfaces in LMBs and solid-state batteries. Our analysis also suggests that W_{adhesion} (of Eq. 4) —measuring the energy cost to separate two materials of a heterogeneous interface— is an important descriptor to evaluate the mechanical stability of interfaces.

In particular, W_{adhesion} should be large enough to avoid interface delamination.[53] Yang et al. demonstrated that for common Li-metal||SE interfaces, a W_{adhesion} of 0.7 J m^{-2} was required to prevent the formation of interfacial voids with the application of external pressure of 20-30 MPa.[29] Recently, Seymour and Aguadero[28] have developed a "bond breaking"

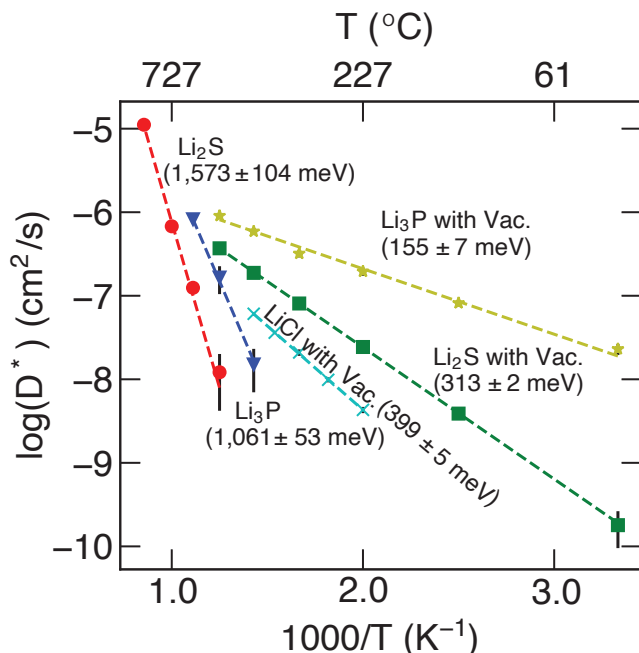


FIG. 3. Arrhenius plots of $\text{Li}^+ D^*$ (in $\text{cm}^2 \text{s}^{-1}$) of bulk binary compounds from MTP-MD simulations. The activation energies, calculated from Eq. 7, and the related error bars are provided as text annotations. Vac. stands for structures with a Li-vacancy.

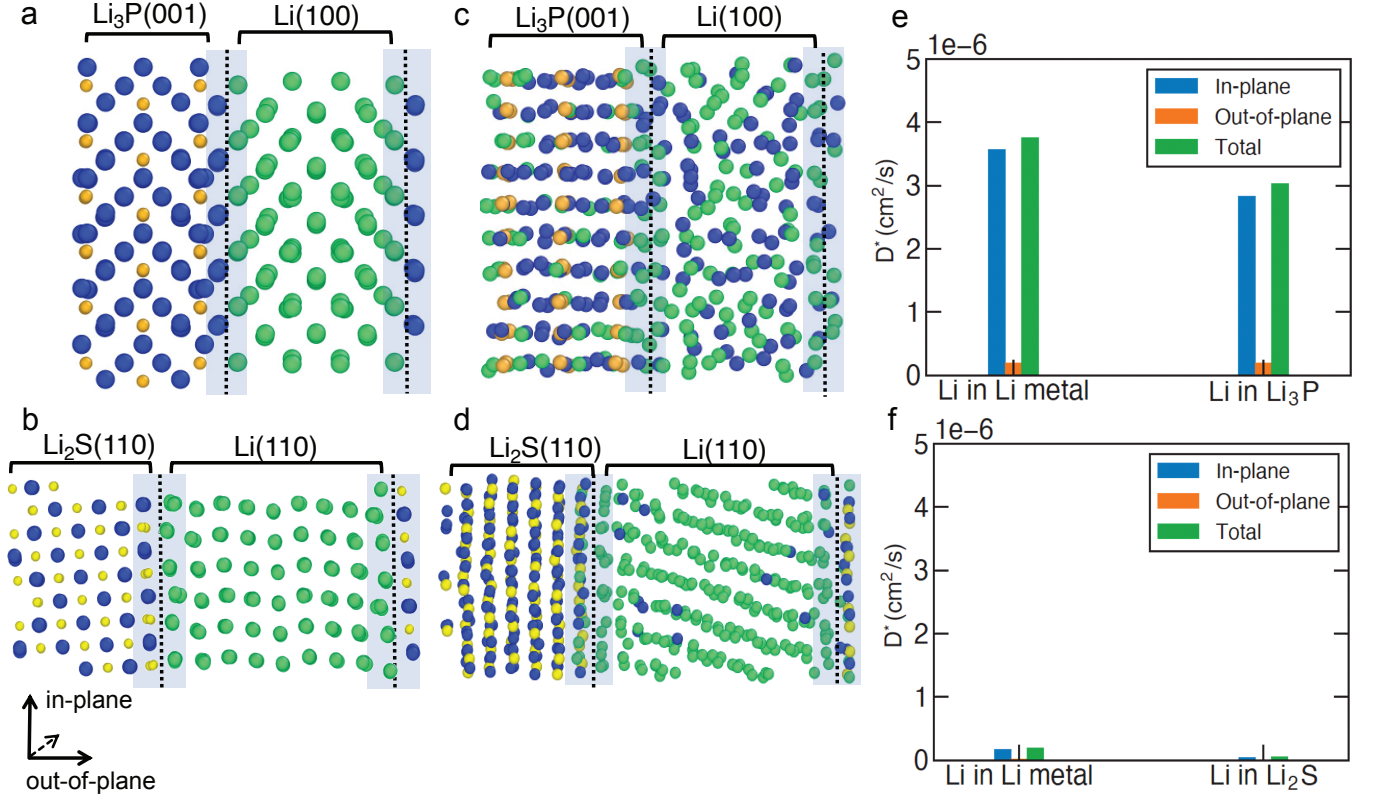


FIG. 4. Snapshots of (a, c) Li(100)||Li₃P(001) and (b, d) Li(110)||Li₂S(110) interfaces at 0 ns (a and b), and 5 ns (c and d), respectively, at 400 K. The in-plane and out-of-plane components of Li⁺-D* in the Li-metal and Li₃P regions (e) of Li(100)||Li₃P(001) interface and Li₂S regions (f) of Li(110)||Li₂S(110) interface at 400 K. Dark blue spheres: Li⁺ (binary), green spheres: Li⁺ (metal), orange spheres: P and yellow spheres: S.

approach and derived that if $W_{\text{adhesion}} > 2\gamma$ (where γ is the surface energy of Li or Na-metal), the formation of interfacial voids with potential loss of contact during the Li (or Na) stripping could be avoided. Our data suggest that among Li-based interfaces (Table S4), only the Li(100)||Li₂O(110), Li(100)||Li₃N(110) and Li(110)||Li₃N(110) interfaces satisfy this criterion. For interfaces with Na-metal, only the two Na||Na₂O interfaces have a W_{adhesion} larger than twice of the surface energy of Na(110) (or Na(100)).

The mechanisms of LiPON passivation of Li-metal has been a matter of debate.[23, 24, 32] Recent studies by Hood *et al.*[23] have indicated that Li₃N and Li₂O distribute uniformly on the surface of the Li-metal, while Li₃P was not in direct contact with Li-metal. In contrast, the study led by the Meng research group had suggested that only Li₃N, Li₂O and Li₃PO₄ could be present in the interfacial region formed between Li-metal and LiPON.[24] Our results show that Li||Li₂O and Li||Li₃N interfaces have better interfacial stabilities than Li||Li₃P, which agree well with the experimental scenario that both Li₂O and Li₃N can be in direct contact with Li-metal, while Li₃P can only exist in the sub-interfacial layer.[23]

It has been established that argyrodite SEs are prone

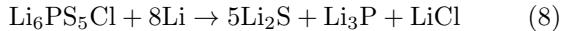
to decomposition against Li-metal,[14, 52] with evidence of formation of Li₂S, Li₃P and LiX (with X=Cl, Br or I) at the potential of Li-metal (i.e., 0 Volts vs. Li/Li⁺). Among the interfaces formed between Li-metal and the decomposition products of argyrodite Li₆PS₅Cl as SE, i.e. Li||Li₂S, Li||Li₃P and Li||LiCl, Li||Li₃P has the largest value of W_{adhesion} (Figure 2), suggesting that Li₃P is more likely to form a stable interface with Li-metal as compared to the other binary compounds. On one hand, the appreciable electronic conductivity of Li₃P could lead to continuous reactions with Li-metal and growth of the decomposing interphases.[54] On the other hand, we have not considered the interfacial stability between binary compounds and Li₆PS₅Cl. Because these interfaces may not be mechanically stable, loss of contact between the SE and its decomposition products may also contribute to increased impedance.[14, 22] Indeed, it has been shown that the change in particle size of Li₂S upon lithiation leads to loss of contact of the Li₆PS₅Cl||Li₂S interface and increases resistance.[25]

The Li⁺ conductivity (or diffusivity) determined in experiments largely depends on the sample quality, its crystallinity and experimental conditions. In particular, the presence of defects, grain boundaries, and lattice disorder all affect the Li⁺ transport significantly.[55, 56] There-

fore, here we have restricted our study to the crystalline structures (both decomposing products and interfaces), a situation where the MTP approach has been proven to be adequate to predict ion transport properties.[52, 57, 58] However, one major limitation of the current implementation of MTP is its lack of transferability from training within the binary bulk systems to being directly used in heterogeneous interfaces, requiring significant retraining of MTP with new training sets for each distinct interface. Therefore, a complete retraining of the MTP for each interface combination considered in this work is highly resource intensive, which pushes a comprehensive examination of Li (and Na) transport across all interfaces out of the scope of our work.

Our MTP results suggest that among the three interface models, the Li-metal||Li₃P displays facile Li transport, as shown in Figure 4c. However, since only the out-of-plane component of Li⁺ diffusivity contributes to the active Li⁺ percolation across the interface, these qualitative results show that the interfaces of Li-metal with Li₃P, Li₂S and LiCl are, overall, resistive to Li-ion transport (Figure 4, Figure S9) compared to the undecomposed argyrodite SE.[52]

Assume that Li₆PS₅Cl reacts entirely with Li-metal (at 0 Volts vs. Li/Li⁺) according to Eq. 8: [14, 15, 52]



where Li₂S is produced 5× in excess over the other binaries, in agreement with experimental evidences.[14, 22] Moreover, from X-ray photoemission spectroscopy (XPS) experiments, Wenzel *et al.* [14] and Schwieter *et al.*[22] have observed the presence of Li₂S, LiCl, and Li₃P at the argyrodite||Li-metal interface. On the basis of our interfacial energetics, Li⁺ transport calculations and Eq. 8, we propose a macroscopic picture of the interface of decomposing argyrodite-Li₆PS₅Cl against Li-metal, as shown in Figure 5.

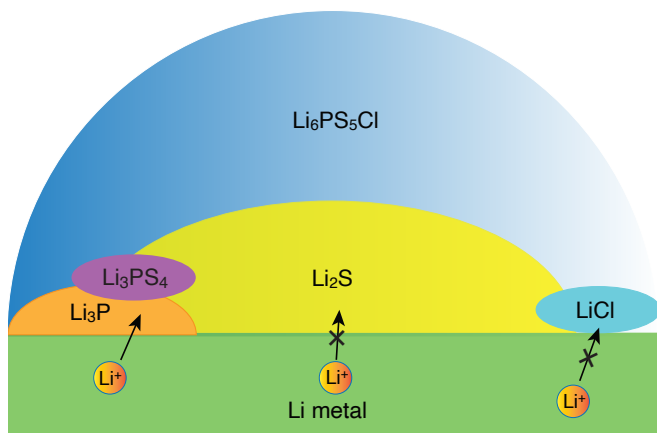


FIG. 5. Schematic illustration of a possible structure of the interface between Li-metal and argyrodite-Li₆PS₅Cl, as inferred from the interfacial energetics and Li-ion transport simulations.

Our data suggests a lower stability of LiCl||Li-metal

interface compared to Li₃P and Li₂S, which indicates that LiCl may be in direct contact with Li-metal over a negligible interfacial area. It appears that LiCl may not be directly involved in interfacial Li-transport. At voltages larger than 0.0 Volts vs. Li/Li⁺ other decomposition products have been reported and observed, with the most prominent being Li₃PS₄,[15, 20, 22] which may form in the sub-interfacial layers of the SE. Furthermore, our MTP-MD demonstrated that Li percolation in the Li||Li₃P interface is facile compared to the other interfaces as signified by the black arrows in Figure 5.

VI. CONCLUSION

Chalcogen-containing SEs show among the highest room temperature ionic conductivities ($\sim 10^{-2}$ S cm⁻¹), but their practical applications in LMBs are limited by the decomposing interfaces when in contact with Li metal. Similar constraints bottleneck the implementation of SEs in NIBs as well. Therefore, it is vital to understand the interfacial properties of these decomposing interfaces, either experimentally or theoretically. In this work, we have systematically evaluated the thermodynamic stability (of Li- and Na-systems) and Li-ion transport properties of multiple decomposing interfaces, by employing first-principles calculations and large-scale MD simulations based on MLPs. Our results reveal that the interfacial stability of decomposition products with alkali-metals is largely affected by the surface properties of the decomposition products. In general, we have observed that the interfaces formed between alkali-metal with argyrodite-Li₆PS₅Cl are resistive, to Li-ion transport. Finally, our high-fidelity MLPs, trained explicitly for interfaces, shed light on the complicated interfacial transport properties, which will aid in the study and optimization of SEs in the future.

VII. METHODS

A. First-principles Calculations

DFT was used to approximate the energy contributions introduced in Sec. II. The wavefunctions were described using plane-waves for the valence electrons together with projected augmented wave potentials for the core electrons as implemented in the Vienna Ab-initio Simulation Package (VASP).[59–61] The exchange-correlation contributions were treated within the generalized gradient approximation (GGA) as parameterized by Perdew, Burke, and Ernzerhof (PBE).[62] The valence electron configurations for each element were as follows: Li: s^1p^0 , N: s^2p^3 , O: s^2p^4 , Na: s^1p^0 , P: s^2p^3 , S: s^2p^4 and Cl: s^2p^5 . The parameters we used for geometry optimization, surface energy and interfacial energetics calculations of the binary compounds and the constructed interfaces follow the MITRelaxSet, as in pymatgen.[63] We used a plane

wave energy cutoff of 520 eV and a k -point mesh generated using a k -point density of 25 \AA^{-1} . The total energy of each structure was converged to 10^{-5} eV/cell, and the geometry optimizations were stopped when the change in total energy was smaller than 10^{-4} eV between two subsequent ionic steps.

AIMD were performed with VASP to generate the initial training sets for the MTP-MD (see Sec. VII B). A plane-wave energy cutoff of 400 eV and a Γ -only k -mesh were used. The canonical ensemble (NVT) was achieved using Nosé-Hoover thermostat and a time step of 2 fs.[64, 65] Since previous studies have reported[57, 66] that the training set for MTP-MD should cover the whole configurational space and contain sufficient data so as to rarely invoke DFT calculations, we performed AIMD calculations at 1000 K for 14-20 ps (preceded by a temperature ramping of 2 ps), which resulted in training sets containing 7000-10000 configurations. The supercell sizes used for binary compounds pristine structures were $4 \times 4 \times 4$ for Li metal (128 atoms), $2 \times 2 \times 2$ for Li_2S (96 atoms), $3 \times 3 \times 3$ for Li_3P (216 atoms) and $3 \times 3 \times 3$ for LiCl (216 atoms). We also studied the vacancy-mediated diffusion by creating Li^+ vacancies inside the Li metal and binary compounds.

Li^+ vacancies were introduced by removing Li atoms and compensating with a uniform (jellium) charge background. Also, we created specific supercells that enabled a Li^+ vacancy concentration of $\sim 0.8\%$ for all compounds, which can arise at a synthesis temperature of 1200 K with a defect formation energy of 0.5 eV. Specifically, we used supercells of $4 \times 4 \times 4$ with one Li^+ vacancy for Li metal (127 atoms), $2 \times 2 \times 4$ with one Li^+ vacancy for Li_2S (191 atoms), $3 \times 3 \times 3$ with one Li^+ vacancy for Li_3P (215 atoms) and $3 \times 3 \times 3$ with one Li^+ vacancy for LiCl (215 atoms). To study the Li^+ transport across Li-metal||decomposition product interfaces, we have created Li^+ vacancies randomly in the interface region (shaded regions in Figures 2 and 4, with a vacancy concentration of $\sim 1.1\%$). The interfaces that we chose were $\text{Li}(110)||\text{Li}_2\text{S}(110)$ (520 atoms), $\text{Li}(100)||\text{Li}_3\text{P}(001)$ (406 atoms) and $\text{Li}(110)||\text{LiCl}(100)$ (439 atoms).

B. Moment-Tensor Potential Molecular Dynamics

MTP for bulk and interfaces investigated in this study were trained using the machine learning of interatomic potentials (MLIP) package.[67] In the training of the MTP potentials, several parameters need to be carefully selected to balance computational cost vs. accuracy of the trained potentials. During training, we have extensively tested the effects of weights on reproducing the *ab initio* total energies, forces and stresses, as well as cutoff radius (R_{cut}) and the maximum level of basis functions (lev_{max}) on the accuracy of energy and forces of trained MTP potentials. We concluded that a ratio of weights of 100:10:1 for energies, forces, and stresses, respectively, was appro-

priate to achieve good accuracy. Also, we found that a lev_{max} of 10 and a R_{cut} of 5 \AA , provided a tolerable level of fitting and validation errors in energies (≤ 10 meV) and forces (≤ 30 meV/ \AA), as documented in Table S6.

Since our MTPs were trained at high temperatures (~ 1000 K), we further validated the transferability of the potentials to lower temperatures (i.e., 300-500 K). Specifically, we constructed validation sets by performing AIMD at 300 K/500 K for 4 ps (~ 2000 snapshots for each temperature). The fitting and validation errors on the total energies in both binary compounds and interface models were always < 10 meV, while the errors on forces were within ~ 30 meV \AA^{-1} .

Upon training, MTP-MD were performed using LAMMPS,[68] where the MD simulations were performed in the temperature range of 300-1000 K at intervals of 100 K. A Nosé-Hoover thermostat was used to simulate the canonical ensemble (NVT).[64, 65] Long MD simulations were carried out for at least 10 ns with a short timestep of 1 fs, preceded by a temperature ramping for 100 ps and an equilibration period of 1 ns to reach each target temperature. We also benchmarked our MTP D^* data with AIMD results (see Table S9). Specifically, we find that our MTP-MD calculated D^* at 900 K and 800 K are in reasonable agreement with AIMD calculations at the same temperatures, signifying the high fidelity of our MTP-MD simulations.

C. Validation of Interfacial Models

To verify the accuracy of our methodology in predicting interfacial properties, we have calculated interfacial energetics using two additional “constrained” optimization methods, namely, *i*) “Fix-binary”: the middle layers of the decomposition product was fixed to mimic the bulk in-plane lattice constants of the binary compound, and, *ii*) “Fix-metal”: middle layers of Li(Na) metal are fixed. The default method used throughout the work is when we do not constrain the middle layers of either binary compounds or the metal, referred to as “Fully-relaxed”. To test these scenarios, we chose $\text{Na}(110)||\text{Na}_2\text{O}(110)$ for Na-based and $\text{Li}(100)||\text{Li}_3\text{P}(001)$ for Li-based interfaces, respectively. The calculated E_f , with and without constrained optimization, are shown in Figure S6. Notably, E_f calculated using constrained optimization is $\sim 0.02 \text{ J m}^{-2}$ and $\sim 0.1 \text{ J m}^{-2}$ higher than Fully-relaxed for $\text{Li}(100)||\text{Li}_3\text{P}(001)$, and $\text{Na}(110)||\text{Na}_2\text{O}(110)$, respectively.

ACKNOWLEDGMENTS

J.W. A.A.P. and P.C. acknowledges funding from the National Research Foundation under his NRF Fellowship NRFF12-2020-0012. The computational work was performed on resources of the National Supercomputing Centre, Singapore (<https://www.nscc.sg>).

* pcanepa@nus.edu.sg

- [1] J. B. Goodenough and Y. Kim, Challenges for Rechargeable Li Batteries, *Chem. Mater.* **22**, 587 (2010), doi: 10.1021/cm901452z.
- [2] W. Xu, J. Wang, F. Ding, X. Chen, E. Nasybulin, Y. Zhang, and J.-G. Zhang, Lithium metal anodes for rechargeable batteries, *Energy Environ. Sci.* **7**, 513 (2014).
- [3] D. Lin, Y. Liu, and Y. Cui, Reviving the lithium metal anode for high-energy batteries, *Nature Nanotech* **12**, 194 (2017).
- [4] T. Krauskopf, F. H. Richter, W. G. Zeier, and J. Janek, Physicochemical Concepts of the Lithium Metal Anode in Solid-State Batteries, *Chem. Rev.* **120**, 7745 (2020).
- [5] X.-B. Cheng, R. Zhang, C.-Z. Zhao, and Q. Zhang, Toward Safe Lithium Metal Anode in Rechargeable Batteries: A Review, *Chem. Rev.* **117**, 10403 (2017).
- [6] C. Fang, B. Lu, G. Pawar, M. Zhang, D. Cheng, S. Chen, M. Ceja, J.-M. Doux, H. Musrock, M. Cai, B. Liaw, and Y. S. Meng, Pressure-tailored lithium deposition and dissolution in lithium metal batteries, *Nat Energy* **6**, 987 (2021).
- [7] K. Xu, Nonaqueous Liquid Electrolytes for Lithium-Based Rechargeable Batteries, *Chem. Rev.* **104**, 4303 (2004).
- [8] N. Yabuuchi, K. Kubota, M. Dahbi, and S. Komaba, Research Development on Sodium-Ion Batteries, *Chem. Rev.* **114**, 11636 (2014).
- [9] P. K. Nayak, L. Yang, W. Brehm, and P. Adelhelm, From Lithium-Ion to Sodium-Ion Batteries: Advantages, Challenges, and Surprises, *Angew. Chem. Int. Ed.* **57**, 102 (2018).
- [10] C. Delmas, Sodium and Sodium-Ion Batteries: 50 Years of Research, *Adv. Energy Mater.* **8**, 1703137 (2018).
- [11] J. Haruyama, K. Sodeyama, L. Han, K. Takada, and Y. Tateyama, Space-Charge Layer Effect at Interface between Oxide Cathode and Sulfide Electrolyte in All-Solid-State Lithium-Ion Battery, *Chem. Mater.* **26**, 4248 (2014).
- [12] H. Tang, Z. Deng, Z. Lin, Z. Wang, I.-H. Chu, C. Chen, Z. Zhu, C. Zheng, and S. P. Ong, Probing Solid-Solid Interfacial Reactions in All-Solid-State Sodium-Ion Batteries with First-Principles Calculations, *Chem. Mater.* **30**, 163 (2018), doi: 10.1021/acs.chemmater.7b04096.
- [13] E. A. Wu, C. S. Kompella, Z. Zhu, J. Z. Lee, S. C. Lee, I.-H. Chu, H. Nguyen, S. P. Ong, A. Banerjee, and Y. S. Meng, New Insights into the Interphase between the Na Metal Anode and Sulfide Solid-State Electrolytes: A Joint Experimental and Computational Study, *ACS Appl. Mater. Interfaces* **10**, 10076 (2018).
- [14] S. Wenzel, S. J. Sedlmaier, C. Dietrich, W. G. Zeier, and J. Janek, Interfacial reactivity and interphase growth of argyrodite solid electrolytes at lithium metal electrodes, *Solid State Ionics* **318**, 102 (2018).
- [15] W. D. Richards, L. J. Miara, Y. Wang, J. C. Kim, and G. Ceder, Interface Stability in Solid-State Batteries, *Chem. Mater.* **28**, 266 (2016), doi: 10.1021/acs.chemmater.5b04082.
- [16] B. Gao, R. Jaleem, and Y. Tateyama, First-Principles Study of Microscopic Electrochemistry at the LiCoO₂ Cathode/LiNbO₃ Coating/ β -Li₃PS₄ Solid Electrolyte Interfaces in an All-Solid-State Battery, *ACS Appl. Mater. Interfaces* **13**, 11765 (2021).
- [17] T. Famprikis, P. Canepa, J. A. Dawson, M. S. Islam, and C. Masquelier, Fundamentals of inorganic solid-state electrolytes for batteries, *Nat. Mater.* **18**, 1278 (2019).
- [18] T. Famprikis, Ö. U. Kudu, J. A. Dawson, P. Canepa, F. Fauth, E. Suard, M. Zbiri, D. Dambournet, O. J. Borkiewicz, H. Bouyanff, S. P. Emge, S. Cretu, J.-N. Chotard, C. P. Grey, W. G. Zeier, M. S. Islam, and C. Masquelier, Under Pressure: Mechanochemical Effects on Structure and Ion Conduction in the Sodium-Ion Solid Electrolyte Na₃PS₄, *J. Am. Chem. Soc.* **142**, 18422 (2020).
- [19] L. Baggetto, R. A. H. Niessen, F. Roozeboom, and P. H. L. Notten, High Energy Density All-Solid-State Batteries: A Challenging Concept Towards 3D Integration, *Adv. Funct. Mater.* **18**, 1057 (2008).
- [20] Y. Zhu, X. He, and Y. Mo, First principles study on electrochemical and chemical stability of solid electrolyte-electrode interfaces in all-solid-state Li-ion batteries, *J. Mater. Chem. A* **4**, 3253 (2016).
- [21] V. Lacivita, Y. Wang, S.-H. Bo, and G. Ceder, *Ab Initio* investigation of the stability of electrolyte/electrode interfaces in all-solid-state Na batteries, *J. Mater. Chem. A* **7**, 8144 (2019).
- [22] T. K. Schwieter, V. A. Arszewska, C. Wang, C. Yu, A. Vasileiadis, N. J. J. de Klerk, J. Hageman, T. Hupfer, I. Kerkamm, Y. Xu, E. van der Maas, E. M. Kelder, S. Ganapathy, and M. Wagemaker, Clarifying the relationship between redox activity and electrochemical stability in solid electrolytes, *Nat. Mater.* **19**, 428 (2020).
- [23] Z. D. Hood, X. Chen, R. L. Sacchi, X. Liu, G. M. Veith, Y. Mo, J. Niu, N. J. Dudney, and M. Chi, Elucidating Interfacial Stability between Lithium Metal Anode and Li Phosphorus Oxynitride via *In Situ* Electron Microscopy, *Nano Lett.* **21**, 151 (2021).
- [24] D. Cheng, T. A. Wynn, X. Wang, S. Wang, M. Zhang, R. Shimizu, S. Bai, H. Nguyen, C. Fang, M.-c. Kim, W. Li, B. Lu, S. J. Kim, and Y. S. Meng, Unveiling the Stable Nature of the Solid Electrolyte Interphase between Lithium Metal and LiPON via Cryogenic Electron Microscopy, *Joule* **4**, 2484 (2020).
- [25] C. Yu, S. Ganapathy, N. J. J. de Klerk, I. Roslon, E. R. H. van Eck, A. P. M. Kentgens, and M. Wagemaker, Unravelling Li-Ion Transport from Picoseconds to Seconds: Bulk versus Interfaces in an Argyrodite Li₆PS₅Cl–Li₂S All-Solid-State Li-Ion Battery, *J. Am. Chem. Soc.* **138**, 11192 (2016).
- [26] N. D. Lepley and N. A. W. Holzwarth, Modeling interfaces between solids: Application to Li battery materials, *Phys. Rev. B* **92**, 214201 (2015).
- [27] C.-T. Yang and Y. Qi, Maintaining a Flat Li Surface during the Li Stripping Process via Interface Design, *Chem. Mater.* **33**, 2814 (2021).
- [28] I. D. Seymour and A. Aguiadero, Suppressing void formation in all-solid-state batteries: The role of interfacial adhesion on alkali metal vacancy transport, *J. Mater. Chem. A*, 10.1039.D1TA03254B (2021).
- [29] M. Yang, Y. Liu, A. M. Nolan, and Y. Mo, Interfacial Atomistic Mechanisms of Lithium Metal Stripping and Plating in Solid-State Batteries, *Adv. Mater.* **33**, 2008081 (2021).

- (2021).
- [30] F. Mizuno, A. Hayashi, K. Tadanaga, and M. Tatsumisago, New, Highly Ion-Conductive Crystals Precipitated from $\text{Li}_2\text{S-P}_2\text{S}_5$ Glasses, *Adv. Mater.* **17**, 918 (2005).
 - [31] T. Hakari, M. Nagao, A. Hayashi, and M. Tatsumisago, All-solid-state lithium batteries with Li_3PS_4 glass as active material, *Journal of Power Sources* **293**, 721 (2015).
 - [32] A. Schwöbel, R. Hausbrand, and W. Jaegermann, Interface reactions between LiPON and lithium studied by in-situ X-ray photoemission, *Solid State Ionics* **273**, 51 (2015).
 - [33] P. W. Tasker, The stability of ionic crystal surfaces, *J. Phys. C: Solid State Phys.* **12**, 4977 (1979).
 - [34] K. T. Butler, G. Sai Gautam, and P. Canepa, Designing interfaces in energy materials applications with first-principles calculations, *npj Comput Mater* **5**, 19 (2019).
 - [35] T. Einstein, Equilibrium Shape of Crystals, in *Handbook of Crystal Growth* (Elsevier, 2015) pp. 215–264.
 - [36] R. Tran, Z. Xu, B. Radhakrishnan, D. Winston, W. Sun, K. A. Persson, and S. P. Ong, Surface energies of elemental crystals, *Sci Data* **3**, 160080 (2016).
 - [37] Y.-X. Chen and P. Kaghazchi, Metalization of Li_2S particle surfaces in Li-S batteries, *Nanoscale* **6**, 13391 (2014).
 - [38] W. C. Mackrodt, Atomistic simulation of the surfaces of oxides, *J. Chem. Soc., Faraday Trans. 2* **85**, 541 (1989).
 - [39] Z. Liu, Y. Qi, Y. X. Lin, L. Chen, P. Lu, and L. Q. Chen, Interfacial Study on Solid Electrolyte Interphase at Li Metal Anode: Implication for Li Dendrite Growth, *J. Electrochem. Soc.* **163**, A592 (2016).
 - [40] A. Hashibon, C. Elsasser, and M. Ruhle, Structure at abrupt copper-alumina interfaces: An ab initio study, *Acta Materialia* **53**, 5323 (2005).
 - [41] R. Benedek, D. N. Seidman, and C. Woodward, The effect of misfit on heterophase interface energies, *J. Phys.: Condens. Matter* **14**, 2877 (2002).
 - [42] A.-L. Dalverny, J.-S. Filhol, and M.-L. Doublet, Interface electrochemistry in conversion materials for Li-ion batteries, *J. Mater. Chem.* **21**, 10134 (2011).
 - [43] N. T. Taylor, F. H. Davies, I. E. M. Rudkin, C. J. Price, T. H. Chan, and S. P. Heplestone, ARTEMIS: Ab initio restructuring tool enabling the modelling of interface structures, *Computer Physics Communications* **257**, 107515 (2020).
 - [44] Z. Deng, Z. Wang, I.-H. Chu, J. Luo, and S. P. Ong, Elastic Properties of Alkali Superionic Conductor Electrolytes from First Principles Calculations, *J. Electrochem. Soc.* **163**, A67 (2016).
 - [45] A. Kato, H. Kowada, M. Deguchi, C. Hotehama, A. Hayashi, and M. Tatsumisago, XPS and SEM analysis between Li/ Li_3PS_4 interface with Au thin film for all-solid-state lithium batteries, *Solid State Ionics* **322**, 1 (2018).
 - [46] Y. Xiao, Y. Wang, S.-H. Bo, J. C. Kim, L. J. Miara, and G. Ceder, Understanding interface stability in solid-state batteries, *Nat Rev Mater* **5**, 105 (2020).
 - [47] J. Bates, Electrical properties of amorphous lithium electrolyte thin films, *Solid State Ionics* **53–56**, 647 (1992).
 - [48] A. V. Shapeev, Moment Tensor Potentials: A Class of Systematically Improvable Interatomic Potentials, *Multiscale Model. Simul.* **14**, 1153 (2016).
 - [49] R. Court-Castagnet, Ionic conductivity-enhancement of LiCl by homogeneous and heterogeneous dopings, *Solid State Ionics* **61**, 327 (1993).
 - [50] G. Nazri, Preparation, structure and ionic conductivity of lithium phosphide, *Solid State Ionics* **34**, 97 (1989).
 - [51] F. Altorfer, W. Bührer, I. Anderson, O. Schärpf, H. Bill, P. Carron, and H. Smith, Lithium diffusion in the superionic conductor Li_2S , *Physica B: Condensed Matter* **180–181**, 795 (1992).
 - [52] C. Wang, K. Aoyagi, M. Aykol, and T. Mueller, Ionic Conduction through Reaction Products at the Electrolyte–Electrode Interface in All-Solid-State Li^+ Batteries, *ACS Appl. Mater. Interfaces* **12**, 55510 (2020).
 - [53] A. Wang, S. Kadam, H. Li, S. Shi, and Y. Qi, Review on modeling of the anode solid electrolyte interphase (SEI) for lithium-ion batteries, *npj Comput Mater* **4**, 15 (2018).
 - [54] P. Gorai, T. Famprikis, B. Singh, V. Stevanović, and P. Canepa, Devil is in the Defects: Electronic Conductivity in Solid Electrolytes, *Chem. Mater.* **33**, 7484 (2021).
 - [55] V. Lacivita, N. Artrith, and G. Ceder, Structural and Compositional Factors That Control the Li-Ion Conductivity in LiPON Electrolytes, *Chem. Mater.* **30**, 7077 (2018).
 - [56] E. Sebt, H. A. Evans, H. Chen, P. M. Richardson, K. M. White, R. Giovine, K. P. Koirala, Y. Xu, E. Gonzalez-Correa, C. Wang, C. M. Brown, A. K. Cheetham, P. Canepa, and R. J. Clément, Stacking Faults Assist Lithium-Ion Conduction in a Halide-Based Superionic Conductor 10.48550/ARXIV.2203.00814 (2022).
 - [57] C. Wang, K. Aoyagi, P. Wisesa, and T. Mueller, Lithium Ion Conduction in Cathode Coating Materials from On-the-Fly Machine Learning, *Chem. Mater.* **32**, 3741 (2020).
 - [58] J. Qi, S. Banerjee, Y. Zuo, C. Chen, Z. Zhu, M. Holekevi Chandrappa, X. Li, and S. Ong, Bridging the gap between simulated and experimental ionic conductivities in lithium superionic conductors, *Materials Today Physics* **21**, 100463 (2021).
 - [59] P. E. Blöchl, Projector augmented-wave method, *Phys. Rev. B* **50**, 17953 (1994).
 - [60] G. Kresse and D. Joubert, From ultrasoft pseudopotentials to the projector augmented-wave method, *Phys. Rev. B* **59**, 1758 (1999).
 - [61] G. Kresse and J. Furthmüller, Efficient iterative schemes for *ab initio* total-energy calculations using a plane-wave basis set, *Phys. Rev. B* **54**, 11169 (1996).
 - [62] J. P. Perdew, K. Burke, and M. Ernzerhof, Generalized Gradient Approximation Made Simple, *Phys. Rev. Lett.* **77**, 3865 (1996).
 - [63] S. P. Ong, W. D. Richards, A. Jain, G. Hautier, M. Kocher, S. Cholia, D. Gunter, V. L. Chevrier, K. A. Persson, and G. Ceder, Python Materials Genomics (pymatgen): A robust, open-source python library for materials analysis, *Computational Materials Science* **68**, 314 (2013).
 - [64] S. Nosé, A unified formulation of the constant temperature molecular dynamics methods, *The Journal of Chemical Physics* **81**, 511 (1984).
 - [65] W. G. Hoover, Canonical dynamics: Equilibrium phase-space distributions, *Phys. Rev. A* **31**, 1695 (1985).
 - [66] I. Novoselov, A. Yanilkin, A. Shapeev, and E. Podryabinkin, Moment tensor potentials as a promising tool to study diffusion processes, *Computational Materials Science* **164**, 46 (2019).
 - [67] E. V. Podryabinkin and A. V. Shapeev, Active learning of linearly parametrized interatomic potentials, *Computational Materials Science* **140**, 171 (2017).

- [68] S. Plimpton, Fast Parallel Algorithms for Short-Range Molecular Dynamics, *Journal of Computational Physics* **117**, 1 (1995).